Rapid heat discharge during deep-sea eruptions generates megaplumes and disperses tephra

Samuel S. Pegler[1] and David J. Ferguson[2]

Deep-marine volcanism drives Earth's most energetic transfers of heat and mass between the crust and the oceans. Seafloor magmatic activity has been correlated in time with the appearance of massive enigmatic plumes of hydrothermal fluid, known as megaplumes, yet little is known of the primary source and intensity of the hydrothermal energy release that occurs during seafloor volcanic events. Consequently the origin of megaplumes remains ambiguous. By developing a model for the dispersal of submarine tephras, we show that the transport of pyroclasts requires an extremely rapid energy discharge, forming a hydrothermal plume with characteristics matching those of megaplumes. Our results show that megaplume formation, which we predict can occur in a matter of hours, is concurrent with lava extrusion. However, the predicted release rate of heat energy considerably exceeds that available from lava alone, giving evidence that syn-eruptive discharges of heated crustal fluids provide the dominant source of megaplume energy. The ubiquity of submarine tephra deposits suggests that powerful ($\sim$1 TW) intervals of hydrothermal discharge must be commonplace during eruptions in the deep-ocean.

INTRODUCTION

Deep-marine volcanism and megaplumes

The vast majority of Earth's volcanism occurs underwater in the deep oceans (>500 m water depth), mostly at ocean ridges and seamounts. Seafloor magmatism accounts for >80% of the global volcanic heat flux [1] and facilitates important chemical-physical interactions between the crust and the ocean. One significant such interaction is the generation of massive (10-150 km^3) ephemeral emissions of hydrothermal fluid termed 'megaplumes' (or large-volume 'event plumes') [2–7] (Fig. 1). Megaplumes are characterized by high ratios of heat to hydrothermal chemical components compared to the plumes produced by chronic hydrothermal vents [7], such as black smokers. Their total energy contents are comparable to the annual thermal output from a typical mid-ocean ridge (MOR) hydrothermal vent field [2], implying extremely high

---

[1]School of Mathematics, University of Leeds, Leeds, LS2 9JT, UK. Email: s.pegler@leeds.ac.uk
[2]School of Earth and Environment, University of Leeds, Leeds, LS2 9JT, UK. Email: d.j.ferguson@leeds.ac.uk
This is a pre-print of a manuscript currently under review with Nature Communications

rates of energy discharge. Oceanographic observations have suggested the existence of a temporal correlation between megaplume creation and deep sea magmatic events [5], most likely with those involving lava extrusion (as opposed to non-eruptive dike intrusions). Despite this apparent association with submarine eruptions, the processes that form a megaplume remain unclear. Several theories exist for the source(s) of megaplume heat contents and fluids. These include: the direct heating of seawater by lava [8]; the evacuation of existing intracrustal hydrothermal reservoirs [2, 7]; the heating and release of crustal fluids by intruded magma [9]; and heat transfer from magma and exsolved volatiles during pyroclastic eruptions [10]. Differentiating between these is challenging because few observations of active deep marine eruptions exist. In particular, while models of the dynamics of megaplumes have suggested that they may form rapidly [11], little is known of the rates of energy or volume discharge feeding the plume during a seafloor eruption, nor of the primary source of the hydrothermal input, nor the role of eruption dynamics on plume formation.

To address these questions, we develop and apply a new model based on utilizing heat-driven tephra transport in the neutrally buoyant umbrella of a hydrothermal plume to constrain the energetics of syn-eruptive heat discharge during deep submarine eruptions. The model enables a novel approach of using buoyancy-driven tephra transport by the umbrella of volcanic plumes to invert for the co-eruptive rate of energy release. By applying the model to a unique dataset of mapped submarine tephra deposits from an MOR eruption [10], we conduct the first inversion of a submarine tephra deposit. The result yields direct predictions for the energy transfer rates associated with co-eruptive plume-driven tephra transport in the deep ocean. Our result shows that the dispersal of tephra over the km-scale distances commonly observed at deep marine volcanic settings requires a rapid syn-eruptive energy transfer, with total inferred energy releases that align precisely with independent oceanographic constraints on both megaplume volume and energy contents. This provides direct evidence that megaplume formation can occur synchronously with the explosive phase of deep-sea eruptions, likely over hours. The predicted rate of co-eruptive energy discharge is large enough that it is highly unlikely to be sourced solely from the erupted magma, and hence we predict that deep-marine eruptions commonly instigate large evacuations of heated fluid from the crust.

Submarine pyroclastic deposits

Observations made over the last decade or so have shown that pyroclastic deposits are a common feature of deep-marine volcanic settings. Imaging and sampling of the seafloor at ridges [10, 14, 15, 21] and seamounts [16–18, 22, 24–26] has revealed the presence of tephra over many km^2, typically in the form of sub-cm shards of volcanic glass with inferred dispersal distances typically reaching several km. Older tephra-bearing sediments recovered from sediment cores taken on the flanks of MORs also indicate similar dispersal scales [19, 20]. In addition, explosive activity has been directly witnessed at water depths exceeding 500 m during eruptions at submerged arc [27, 28] and rear-arc [29] volcanoes. Together, these observations run contrary to the previously long-held view that energetic, explosive-style eruptions are rare in the
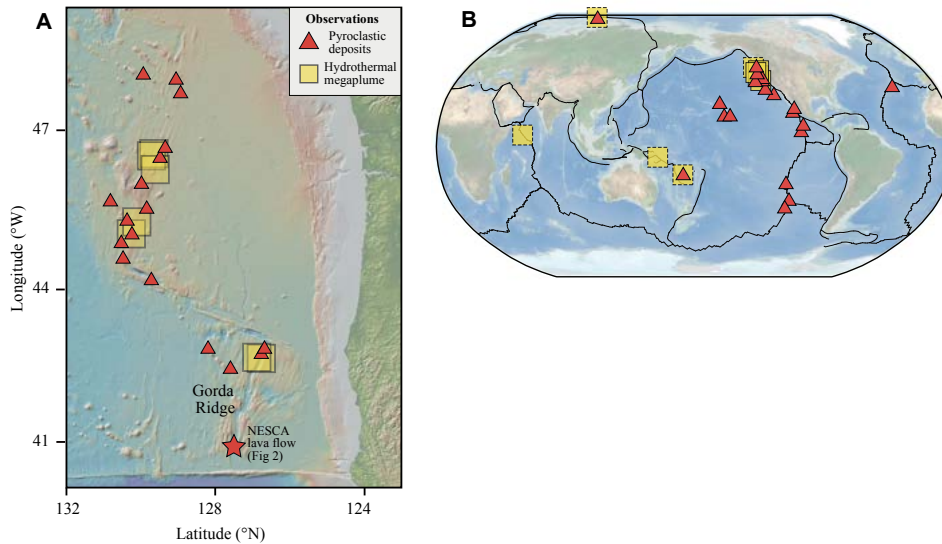
Figure 1: **Observations of hydrothermal megaplumes and deep-marine tephra deposits.** Locations of megaplumes detected by water-column measurements (yellow boxes) and observed deep-marine pyroclastic tephras (red circles) in (A) the NE Pacific and (B) globally. Boxes with solid lines show plumes that have been mapped in three dimensions and therefore have known volumes ($\sim$10-150 km^3), while dashed lines indicate those with chemical and physical characteristics consistent with a megaplume but without a confident volume estimate. Deep-marine tephras have been discovered in multiple locations at both MORs and seamounts. These encompass the global range of MOR spreading rates and water depths of up to 4 km. The preponderance of observations in the NE Pacific (shown in (A)) is related to the concentration of marine research in this region. The location of the eruption and tephra deposit used for our inversion (Fig. 2) is shown by the star symbol in (A)). Tephra observations, particularly in (A), are from [10] with additional data from [14–22]. Megaplume observations are from compilations by [5, 6]. Black lines in (B) show tectonic plate boundaries.

deep ocean in light of the predicted suppression of explosive processes by hydrostatic pressure [30]. Instead, the generation and dispersal of pyroclasts, of both silicic and basaltic composition, appears to be common during deep-marine eruptions. However, with the exception of the pyroclastic deposit studied here (sampled and mapped by [10]), no detailed information exists on the distribution of submarine tephras around their source eruptive vent or fissure, the location of which is typically unknown. As such, the development of an explanation for the primary mechanism of tephra dispersal, as well as the assessment of the possibility to invert submarine depositional patterns for paleo-eruptive properties (as is routinely done for subaerial tephras [32]), have remained unexplored to date.

The inversion methodology we develop uses the buoyancy-driven flow of a particle-laden plume umbrella formed during a submarine eruption to form a constraint on the volume flux
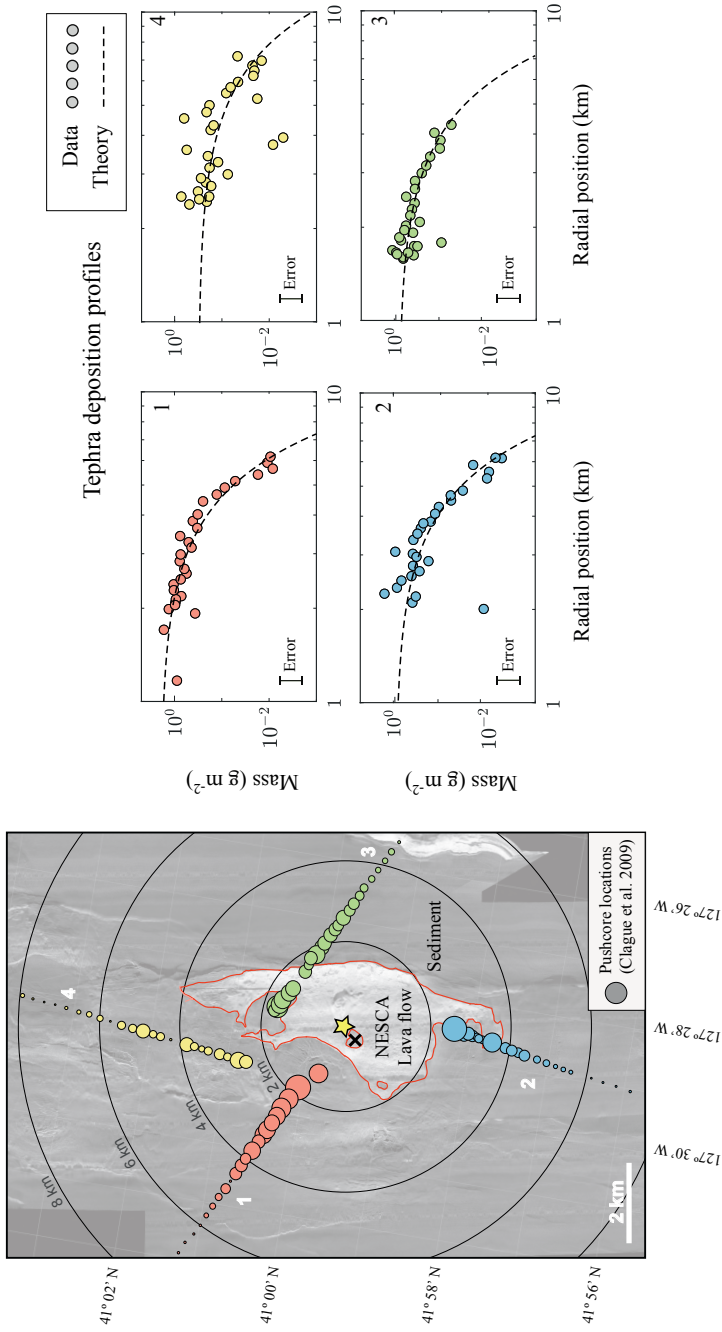
3

Figure 2: **Map and tephra deposition pattern at the NESCA eruption site with theoretical fits.** (A) Sidescan sonar imagery of the NESCA lava flow at the southern end of the Gorda Ridge (see Fig. 1A). Circles show locations of sediment pushcores taken along four profiles around the flow by [10], with the area of the data points proportional to the mass per unit area of tephra in the 250-500 μm range. The extent of the lava flow is indicated by a red outline. Plots to the right show the mass per unit area of the corresponding sampled data profiles (labeled 1-4) as a function of distance from an inferred positions of the source vent, marked by the yellow star in the map. The inferred center is the unique position such that the regression of profiles 1-3 predict the same dispersal length (profile 4 was deemed too scattered to be used). This is almost indistinguishable from the location of the actual eruptive vent, recently identified using high-resolution bathymetric data (D. Clague, pers. commm.) and shown by the black cross. Least-squares fits of the theoretical Gaussian dispersal pattern for umbrella-driven dispersal are shown as dashed curves on the plots. From these fits, the dispersal scale $L \approx 4.7$ km is inferred. Concentric circles represent 2-km increments from the calculated center. Sonar imagery from [23].

feeding it and, in turn, the seafloor energy flux. The model differs fundamentally from those typically used for inversion of tephras from subaerial eruptions in that it utilizes a model of the neutrally buoyant umbrella component of the plume explicitly, of the kind considered experimentally and theoretically in the laboratory by [38], to invert for the flux of plume fluid reaching the neutral level. The umbrella region maintains particles in turbulent suspension whilst spreading laterally under buoyancy. These dynamics are typically neglected in inversion methodologies developed for subaerial eruptions [32], where horizontal transport is assumed to be controlled instead by advection by crosswinds and diffusion by atmospheric mixing during ash descent. Our model assumes instead that the dispersal is driven by horizontal buoyancy-driven spreading.

METHODS

Tephra deposit and dispersal characteristics

In this study we formulate a model of particle dispersal by a hydrothermal plume and apply it to invert directly for the energy discharge rates produced during a submarine eruption. This application is possible owing to the existence of a unique dataset of tephra deposition from an isolated submarine eruption, the basaltic Holocene NESCA lava flow [23], collected by D. Clague and co-workers [10] in the Northern Escanaba Trough at the Gorda Ridge, NE Pacific (Fig. 2a). Pyroclasts up to 1000 μm in size, were sampled and mapped around this lava flow, revealing lateral transport to distances exceeding 5 km in all directions from the eruption site. Analysis of the clasts has indicated that the fragments of basaltic glass, which commonly preserve fluidal textures, originated predominantly from magma fragmentation during explosive discharge [10, 14]. Although secondary processes, such as thermal granulation [36], may have also affected the clasts, it should be noted that the precise mechanism of particle generation has no effect on the results of our model (see below). The plots of Fig. 2 show the mass distribution of pyroclasts in the 250-500 μm range along each of four profiles of pushcore data from [10]. In all cases, the mass of material decreases with distance from the source with an approximately axisymmetric, qualitatively Gaussian thinning trend.

It has been suggested that the lateral transport of submarine tephra may be a consequence of vertical lofting, followed directly by settling within a sustained cross current [34]. While tidal oscillations could, in principle, produce a radial-like dispersal, the mechanism cannot account for the Gaussian-like axisymmetric thinning trends of the kind observed at NESCA (see Supplementary Information). We propose instead that the characteristics of the observed tephra deposition suggest a dominant transport mechanism by advection within the *umbrella* of the plume, which forms a buoyancy-driven turbulent intrusion spreading radially along a neutral level.

With no sustained unidirectional cross current, the umbrella would remain approximately axisymmetric during the tephra dispersal phase, advecting particles laterally by its own buoyancy-driven flow whilst maintaining the particles in suspension within turbulent eddies. The heavy

tephra particles gradually fall out of the suspension of the turbulent flow, producing a thinning deposition of tephra in all directions. This proposed mechanism aligns with the observation of a near-axisymmetric dispersal pattern at NESCA, as well as observations of approximately 'ellipsoidal' megaplumes [6, 37]. An axisymmetric umbrella is often considered as an idealized prototype in fluid-mechanical analysis of particle dispersal by subaerial eruptions [38]. However, it is rare in the subaerial context owing to the dominance of prevailing atmospheric crosswinds [39–42], even for the strongest eruptions [32]. Models and inversion toolkits developed for subaerial dispersal [40, 41] typically neglect the buoyancy-driven dynamics of the umbrella region compared to direct advection of settling particles in crosswinds and diffusive mixing. However, buoyancy-driven spreading is the only mechanism that can account for axisymmetric or lateral spreading of the neutrally buoyant flow of the umbrella (even an upper bound on oceanic diffusive mixing near MORs of $\kappa \sim 10^{-2}$ m^2 s^{-1} can account for at most a few 100s m of additional lateral spread during particle descent), and thus we propose that buoyancy must provide the primary driver of the dispersal of tephra in the absence of crossflow.

An input of heat at the seafloor, either by direct lava heating or from the release of hot intracrustal fluids, will coalesce into a vertically convecting column of heated water, herein referred to as the *stem*. This structure will both grow laterally and cool as it entrains ambient seawater until reaching a neutral level at which the density matches that of the ambient stratification (see Fig. 3). Following an inertial overshoot, the plume will settle along the neutral level as a turbulent, primarily horizontally flowing, buoyancy-driven intrusion, forming the *umbrella* of the plume. Tephra produced during eruption of the lava will be carried by the plume stem into the umbrella (a discussion of the condition on the particle settling speed v necessary for the majority of a given particle species to reach the umbrella, as well as the relative significance of dispersal below the stem versus the umbrella, is provided in the Supplementary Information, where a dimensionless number v^4/NF_0 is shown to provide an index for measuring which is dominant in a given situation). The particles will subsequently be transported horizontally within the intrusion, resulting in km-sale lateral transport. This mechanism of transport does not rely on oceanic currents, and is driven independently by the heat energy inputted at the source of the plume.

In a deep-ocean environment, we propose that the transport of tephra both within the umbrella and during settling outside the plume can be influenced by three primary effects. One is lateral advection by buoyancy forces in the umbrella, discussed above. A second is the advection of the plume-particle system (including settling particles) by a sustained deep oceanic current. A third is advection by tidal currents, which imposes a periodic, cyclic advection of the plume-particle system.

Depending on location, the background flow in the deep sea can be anticipated to form from a superposition of deep ocean currents (streams and associated eddies), tidal currents, mesoscale eddies, internal waves and turbulent mixing (e.g. breaking internal waves). Sustained unidirectional currents are likely to be important in regions that contain deep-ocean currents and form part of the global ocean circulation. In view of the near-axisymmetric form of the observed dispersal pattern at NESCA, we can anticipate that advection in a sustained cross flow of this
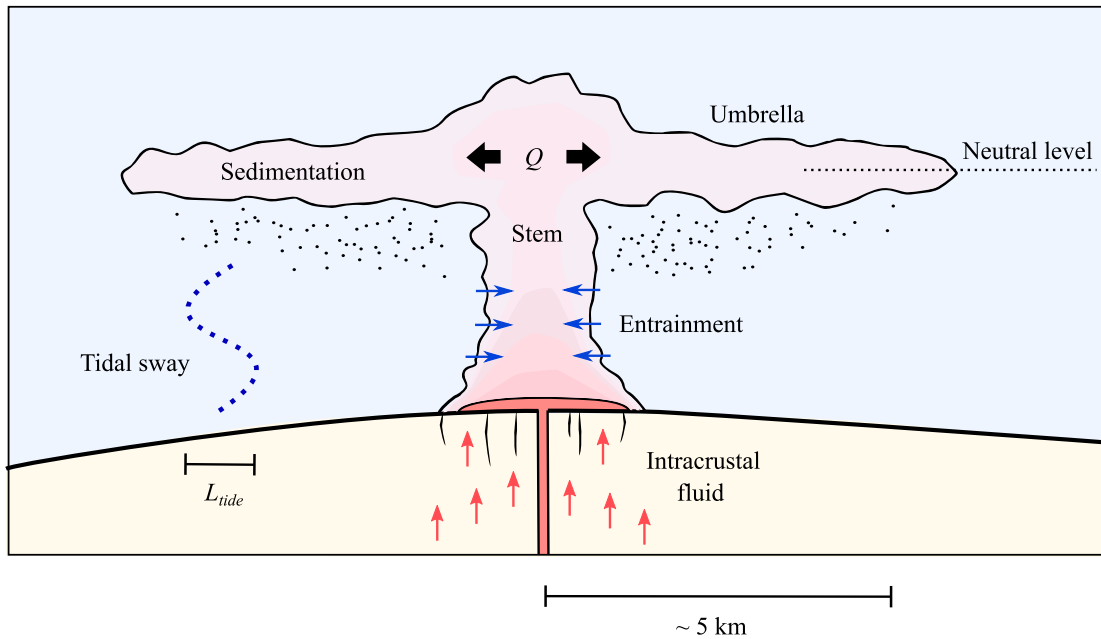
6

Figure 3: **Schematic of processes controlling buoyancy-driven submarine tephra dispersal.** The hydrothermal plume forms a turbulent convecting stem fed by lava heating, and/or release of intracrustal fluid, which accumulates and cools following entrainment of ambient seawater. The stem feeds the neutrally buoyant umbrella, which forms a primarily horizontally flowing intrusion within the density stratification of the ocean, with a volumetric flux of Q. The plot illustrates the predominantly axisymmetric shape with an indication of the spatial scale of tidal oscillation $L_{tide} < 1$ km, compared to the scale of the dispersal (~ 5 km).

kind is highly unlikely in this case. Otherwise, the dispersal would be preferentially skewed in one direction. The lack of a dominant control by sustained cross flows in the NESCA ash deposit is consistent with the absence of focused oceanic currents in the NE Pacific [43]. Like the ash deposition pattern, strong oceanic currents would, in analogy with subaerial umbrella plumes, produce a slender, near-linear plume in the direction of the background crossflow. Observations of several megaplumes have indicated ellipsoidal forms [6, 37] and, in these cases, ocean currents were unlikely to have played a dominant role during their formation. Sustained cross flows in the deep ocean may be primarily localized to regions forming part of the global ocean circulation.

Tidal currents could, in principle, produce a radial-like dispersal, owing to their periodicity. As tidal currents cycle over the course of a diurnal, semi-diurnal or mixed tidal pattern, the plume and settling particles will sway back-and-forth cyclically over the period of the tidal forcing. By considering the trajectories of particles in a tidal field shown in the Supplementary
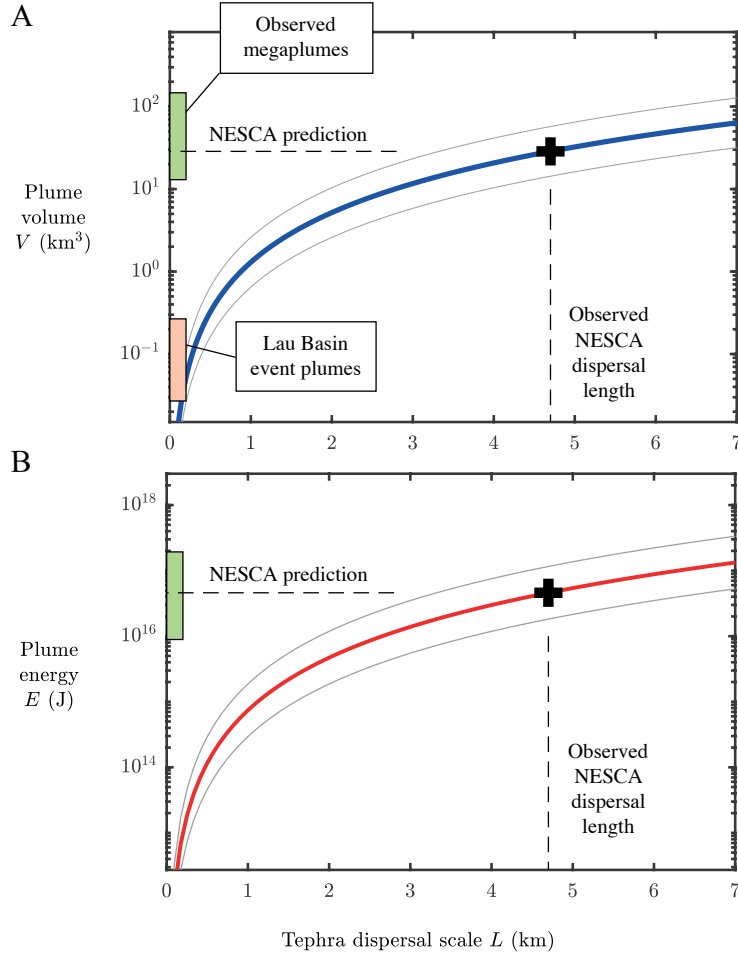
7

Figure 4: **The inversion for plume umbrella volume and total energy and comparison with observed event plumes**. (A) The total volume and (B) total energy predicted by our model (see Supplementary Information for details) as functions of the observed tephra dispersal length scale (L). The value used for the Brunt-Väisälä frequency is $N = 10^{-3}$ s^{-1} and the eruptive time scale was assumed to be $\tau = 12$ hours (see text). The thick curves are evaluated for a settling speed $v = 3$ cm s^{-1}, which represents the particle range 250-500 µm used in the inversion. The other curves (black, thin) represent the inference that would apply for different settling speeds of $v = 1.5$ and 6 cm s^{-1}, to illustrate how different inversion curves arise for different species of particle. The black cross represents the inferred value given the observed dispersal distance of $L = 4.7$ km determined from the fitting of the predicted guassian dispersal profile using the equation given in the text onto the observed data for the NESCA eruption (Fig. 2). Our predictions for the volume and energy content of the plume produce during this eruption are shown as a black cross. The range of volumes and heat energies of observed megaplumes (volume ≥ 10 km^3) [5] are indicated by the green bars, showing consistency with our prediction. This indicates that a megaplume was produced during the NESCA eruption. The volume range of the considerably smaller group of event plumes observed at the Lau Basin [6] are indicated by the red rectangle, potentially forming a distinct category of event plume.

Information, we determine that the dispersal can be constrained geometrically by the upper bound $L_{tide} = UT/2\pi$, referred to as the tidal dispersal scale, where U is the maximum daily speed of tidal flow during the tidal cycle and T is the duration of one day. The length scale L_{tide} represents the maximum distance that can be propagated by a fluid element before the tide reverses during the tidal cycle. For typical maximum tidal flow speeds of ~ 5 cm s^{-1} for the NESCA region (determined using Argo floats [43]), the maximum radius of the orbit is $L_{tide} \sim 700$ m. The much larger dispersal radii of > 5 km observed in all directions at NESCA therefore support a hypothesis that particle transport was dominated by advection within the laterally expanding, buoyancy-driven umbrella of a hydrothermal plume.

Hydrothermal plume model and inversion

We propose that the most plausible mechanism for generating the observed deposition pattern at NESCA is advection within the neutrally buoyant flow created by a thermal discharge during the eruption. If this is the case, then the driver of the dispersal is controlled by the rate of thermal input. In principle, it should therefore be possible to correlate tephra deposition distances with energy input rates, yielding an inroad for the estimation of spatial, temporal and energetic characteristics of discharges produced during either contemporary or paleo deep-sea eruptions.

We consider the buoyancy-driven flow of the eruptive plume in two components, illustrated in Fig. 3, representing two distinct fluid-mechanical regimes. The stem of the plume is modelled as a turbulent, vertically convecting column of hot water, while the umbrella is modelled as a turbulent gravity current flowing along a neutral level of the ambient density stratification (Fig 3) (see Supplementary Information for full model description). The two regions are coupled by a condition of continuous volumetric flux between the top of the stem and the radial origin of the umbrella at the neutral buoyancy level. Particles entrained into the plume will, following possible fallout and recycling in the stem, propagate into the plume umbrella and sediment from its base at a rate proportional to particle concentration [38, 44].

The volcanic contribution to the dispersal is, in accordance with established theory of particle sedimentation from axisymmetric gravity currents [38], a Gaussian pattern, $m(r) = m_0 \exp\left[-\pi(r/L)^2\right]$, where $m(r)$ is the deposited particle mass per unit area (a proxy for tephra thickness), v is the particle settling speed, $L = (Q/v)^{1/2}$ is the volcanic dispersal scale, Q is the volume flux feeding the umbrella, and m_0 is a reference constant (see Supplementary Information). The dispersal length L is independent of both the duration of the eruption and the rate of input of particles (either of which will only accumulate m_0) and hence L provides an independent measurement that can be used to constrain the volumetric flux sourcing the umbrella via the formula $Q = vL^2$ (even a small particle input can be sufficient to conduct this inversion). Utilising further relationships between Q and the plume energetics (see Supplementary Information), we infer the flux of heat energy sourcing the plume, $\Phi = k\left(N^5 Q^4\right)^{1/3}$, where $k \approx 1.82$ GW m^{-4} s^3 is the conversion factor between heat and buoyancy for water, and N is the Brunt-Väisälä frequency. The relationships for Q and Φ given here are general, and allow rates of umbrella growth and hydrothermal heat input to be inferred from observation of

9

the tephra dispersal scale L. Total volume V and energy E implied by these relationships are plotted as functions of L in Fig 4 for an input time scale of $\tau = 12$ hours (estimated for NESCA below).

RESULTS

Dispersal of the NESCA tephra

For the NESCA flow, the observed profiles of tephra deposition (the plots of Fig. 2) follows the predicted Gaussian trends for axisymmetric dispersal in all directions. This supports our essential hypothesis that buoyancy-driven flow in the umbrella was the primary driver of the dispersal. Three of the four profiles shown in Fig. 2 provide a good least-squares fit to the predicted Gaussian structure discussed above on treating the reference constant (m_0) and the volcanic dispersal length-scale (L) as fitting parameters (see equation above and Supplementary Information). Dispersal profiles 1-3 provide almost identical values for $L \approx 4.7$ km for an origin shown as a yellow star in the map of Fig. 2. Profile 4 is too scattered for a statistically significant fit. The scatter in this and the other profiles could be attributable to the effects of aggregation during settling, statistical noise in the turbulent and particle dynamics and/or post-depositional disturbance of the tephra by sediment displacement or bioturbation. The inferred center of the eruption, marked by the yellow cross in Fig. 2, was determined systematically by finding the unique position for which the fitting of the three profiles 1–3 predict the same value of L. Recently acquired high-resolution bathymetry of the NESCA flow (D. Clague, pers. comm.) shows that the source vent lies < 300 m from our inferred center (see Fig 2). This close agreement supports our proposed theoretical explanation for the dispersal through buoyancy-driven axisymmetric spreading in the intrusion, and also indicates the potential to identify source vents from tephra data.

In addition to L, the other parameter required to conduct the inversion is the representative settling speed for the particle species 250–500 µm under consideration. For this we use the general formula for particle settling speeds [33] with coefficients for settling tephra particles determined using tank experiments by [34] (see Supplementary Information for details on these relationships, as well as a discussion of how a representative particle size for a polydisperse particle distribution is defined). The representative settling speed for this group is determined as $v \approx 3 \pm 1$ cm s^{-1}.

Using the mutually consistent dispersal scale of $L = 4.7$ km and the settling speed $v \approx 3$ cm s^{-1}, we infer the volumetric rate of growth of the umbrella to be $Q = vL^2 \approx 2.4$ km^3 hour^{-1} (see Supplementary Information). The corresponding rate of heat transfer inferred to have occurred at the hydrothermal source (ϕ) is predicted to be $\approx 3.8 \times 10^{15}$ J hour^{-1} or, equivalently, 1.1 TW. For this, we used a value for the Brunt-Väisälä frequency (N) of $\approx 10^{-3}$ s^{-1} derived for the seafloor near the NESCA site (see Supplementary Information) using the dataset of [35]. These values of the flux feeding the umbrella Q and the energy input rate at the plume source Φ present estimates for the rates of umbrella growth and heat energy input rates

10

derived directly from the tephra-dispersal dynamics.

Using the relationship between morphology of a submarine lava flow and its rate of effusion [48], one infers an effusion rate for the NESCA flow of $\sim 10^3$ m^3 s^{-1} (see Ref [23, 10]), indicating an eruptive time scale of $\tau \sim 12$ hours. This characteristic duration aligns with estimates of megaplume discharge rates extending over a period of several hours [6]. Based on our direct constraints on volume flux Q and heat transfer rate Φ determined from the tephra deposition pattern above, we estimate that an eruption of this duration would generate a megaplume with an initial volume of ~ 30 km^3 containing $\sim 5 \times 10^{16}$ J of heat. Both of these values are in good agreement with observations of megaplumes suspected to be formed during MOR eruptions (shown as green bars in Fig. 4). This correlation supports a direct causal link between the generation of a megaplume and km-scale dispersal of tephra in the oceans. The predicted volume lies in the lower size range of observed megaplumes while the energy is approximately in the middle, potentially owing to the volumetric growth of megaplumes caused by oceanic diffusive mixing during the period between plume formation and observation.

Sources of megaplume energy

Using the total erupted mass of the NESCA flow of $\sim 1.2 \times 10^{11}$ kg [10]) and using the lava cooling model of [6], we estimate that the total heat energy available from cooling the erupted magma to the temperature of the ambient seawater was $\sim 5 \times 10^{16}$ J. Due to the rapid formation of an insulating crust over the erupted lava [49], only a fraction of this total energy (likely at most 30%) could have contributed to heating of the seawater during the eruption (see discussion in [6]). Although cooling of pyroclasts is more efficient than lava, these only represent <1% of the total erupted mass [10] and cannot therefore be a significant source of heat. Thus, we anticipate that $< 1.5 \times 10^{16}$ J of energy was likely available from the heating of seawater by lava during the eruption. While it has been argued that efficient heating by lava can create megaplumes [8], this is unlikely to have been the dominant mechanism in this case owing to the discrepancy between the most conservative estimate for the energy available from cooling lava ($< 1.5 \times 10^{16}$ J) and the energy necessary for the 5-km-scale dispersal of tephra ($\sim 5 \times 10^{16}$ J). Our direct constraints on the energy discharge rate demonstrate that the heat transfer associated with megaplume formation was significantly more rapid than that expected from cooling of erupted lava [6, 8]. This is consistent with the hypothesis of [6] who also noted a mismatch in total energy contents between observed megaplumes and their associated lava flows. The most obvious source of the additional heat required to form a megaplume is the release of heated intracrustal fluids, either from the sudden evacuation of an existing hydrothermal system [2] or, alternatively, due to the thermomechanical effects of dyke emplacement in the shallow crust [9]. Our results shows that this fluid release must have occurred concurrently with the eruption.

It may be possible to distinguish between the specific source of crustal fluid (hydrothermal reservoir versus heated pore fluid) based on the chemical-physical properties of megaplumes (see [6] and [13] for further discussion), however the spatial-temporal correlation between the appearance of megaplumes and seafloor eruptions (discussed below) favors the latter, as it does

11

not restrict megaplume generation to the location of existing large hydrothermal reservoirs. A crustal origin for at least a portion of megaplume fluids is also consistent with the presence of thermophillic microbes observed in plume fluids at the Gorda Ridge in 1996 [12], suggesting that megaplumes may facilitate the spread of, and provide a means to sample, crustal biota.

Thus, while heating of seawater by erupted magma must provide some component of the immediate co-eruptive heat flux (dependent on mass eruption rate and emplacement style), both the magnitude and rapidity of the heat transfer required for megaplume formation and tephra transport strongly supports an additional, and likely dominant, contribution from heated crustal fluids. Seafloor eruptions that do not involve the concurrent release of significant volumes of crustal fluids, perhaps due to a lack of available fluid or magma ascent conditions that do not promote fluid heating/discharge, should therefore produce substantially smaller plumes. The size of such plumes is limited by the more restricted/short-lived energy transfer available from lava-heating. This may, for example, explain the formation of a series of event plumes of considerably smaller volumes $V < 0.5$ km^3 (indicated as a red bar in Fig. 4 A) detected after an eruption in 2008 in the Lau Basin [6]. It is notable that megaplumes have thus far only been observed, or suspected, above volcanoes in extensional tectonic settings (i.e. MORs and back-arc ridges; Fig. 1), where a porous and permeable uppermost volcanic crust and the presence of faults and fractures formed due to tensile stresses facilitate fluid inflow to the crust. Although future observations may yet document megaplumes associated with other submarine volcanic environments, it could be expected that syn-eruptive plumes in non-rift settings are typically less energetic. This inference could be tested by applying our inversion method to plume dispersed pyroclasts from other submarine volcanic settings (see below), such as submerged volcanic arcs (e.g. [24])

Linking megaplumes, seafloor eruptions and tephra transport

The release of hot intracrustal fluid triggered by magma intrusion does not, in principle, necessitate an eruption. However it is notable that observed megaplumes are commonly associated with events involving lava extrusion [13] and appear to form directly above freshly emplaced lava flows [31]. It has also been noted that, on occasions when seafloor seismic events have not culminated in eruptions, no anomalous hydrothermal activity has been detected [13]. As demonstrated here, in the absence of strong unidirectional currents, achieving transport distances in excess of 1 km for even relatively small pyroclasts (<500 µm) requires a significant time-averaged energy flux close to the eruptive source of around 1 TW. Maintaining this heat flux for a period exceeding 10 hours would equate to a total energy release consistent with the observed heat contents of megaplumes (10^{16}-10^{17} J), shown in Fig. 4B. The apparent ubiquity of widely dispersed submarine tephras (Fig. 1), and the aforementioned correlation between lava extrusion and megaplume detection, both indicate that syn-eruptive energy transfers of a magnitude comparable to that predicted for the NESCA eruption are an intrinsic characteristic of many volcanic events occurring in the deep oceans. In light of this, we anticipate that the processes leading to rapid intracrustal fluid release (i.e. dyke intrusion into the uppermost

crust) will also generally produce lava extrusion, even though the energy from erupted lava alone cannot account for observed tephra transport distances of several km.

The mechanism of tephra-transport through buoyancy-driven flow of the intrusion layer of a dispersing hydrothermal plume that underlies our model can be anticipated to apply in all situations where the background flow is sufficiently quiescent that it is unable to compete significantly with the buoyancy-driven radial flow during particle dispersal. Tephra transport from submarine eruptions can also occur via other mechanisms, such as density currents generated by plume collapse [24, 28] or the advection of settling particles by tides (see Supplementary Information) and ocean currents [34], however these will not produce radially dispersed deposits over length-scales of several km with axisymmetric Gaussian thinning trends (as are clearly apparent in the NESCA data; Fig. 2).

Although in the case investigated here our analysis reveals ash transport within a megaplume, our method is equally applicable to tephra transported by any eruptive plume, regardless of size or total energy content, as long as buoyancy forces dominate dispersal. In situations where background crossflow also contributes, our methodology could be generalized to address this case by comparing observed tephra depositions alongside an umbrella model suitably generalized to incorporate background flow and fitting for the background flow rate and flux feeding the umbrella simultaneously. The signature of the flux feeding the umbrella and, in turn, the heat flux at the seafloor origin, will manifest in the lateral buoyancy-driven expansion of the flow perpendicular to the direction of the crossflow. Our method differs conceptually from the inversion methods typically used for subaerial eruptions [32] where convective and diffusive atmospheric transport processes are used to infer the rise height of ash particles and, in turn, the eruption energy using the stem model of [47]. This method assumes that lateral dispersal occurs in response to background diffusion, and thus would fail in situations where buoyancy-driven flow drives the umbrella, as is likely to be the case here. The method we develop also differs in that it infers the flux feeding the umbrella directly. Thus, our method has the advantages of incorporating the potentially dominant driver of horizontal tephra transport (buoyancy-driven flow of the umbrella), necessary to explain the observations at NESCA, whilst circumventing any need to infer the rise height of the plume.

SUMMARY

We have shown that km-scale tephra dispersal in the deep ocean can be explained by transport in the umbrella of a co-eruptively produced megaplume. The work has demonstrated how the inversion of plume-transported tephras, in this case from a submarine deposit, can be used to to constrain the energy discharge rates associated with volcanic eruptions. Our method presents a novel approach to use transport via buoyancy-driven flow of the umbrella to invert for eruptive energetics. Due to the lack of sustained cross-flows (i.e. strong currents) in many parts of the oceans, plume-transported submarine tephras are likely to be more amenable to this type of inversion relative to their terrestrial counterparts, where atmospheric winds tend to dominate dispersal. In the case of the NESCA eruption, megaplume generation must have occurred concur-

rently with the generation of pyroclasts, as the km-scale axisymmetric dispersal characteristics of this deposit requires the buoyancy-driven mechanism provided by an energetic hydrothermal megaplume. Our results therefore conclusively link the generation of a megaplume with the eruptive phase of a seafloor magmatic event. The similarity between the NESCA tephra deposit and many other deep marine tephras (wrt. particle size, morphology, dispersal range etc.) suggests that this is a common occurrence during submarine eruptions at ocean ridges. The inference that much of the syn-eruptive hydrothermal energy release owes it provenance to crustal sources, suggested here and by others [2, 6, 7, 9, 13], can potentially be tested by future *in situ* observations of syn-eruptive hydrothermal processes [50] and continued sampling and chemical analysis of megaplume fluids. Application of our inversion method to paleo-tephra deposits recovered from marine sediment cores [19, 20] could, in principle, provide new inroads towards constraining the long-term ($\gtrsim$10 ka) time-averages of co-eruptive heat outputs during MOR eruptions.

Supplementary Information

Hydrothermal plume model

The *stem* of the plume forms a turbulent column of hot water that propagates vertically within the ambient density stratification of the ocean. The turbulent flow in the stem of the plume will entrain ambient seawater, causing it to cool and, above a certain height, become heavier than the ambient fluid. Following an inertial overshoot, the flow will settle along a neutral level, forming the *umbrella*. This second regime forms a turbulent, horizontally propagating flow known as an intrusion or (neutrally buoyant) gravity current [42]. The stem and umbrella are coupled by a condition of continuous volumetric flux Q between the top of the stem and the radial source of the umbrella at the neutral buoyancy level. Particles entrained into the plume will, following possible fallout and recycling in the stem, propagate into the plume umbrella and sediment from its base at a rate proportional to particle concentration [38, 44].

We develop a method that inverts observed deposition distances to rates of energy discharge at the seafloor origin of the plume. Our inversion is performed in two steps, working backwards from the deposition, through the umbrella to the plume stem and, finally, to the source vent. The first step uses the observed ash deposition field to infer the volumetric flux feeding the umbrella at the top of the plume stem, denoted by Q and illustrated in figure 3. The second step uses this inference of the flux Q to invert in turn for the rate of heat transfer inputted at the base of the stem, denoted Φ. For the first step, we consider the tephra transport dynamics driven by buoyancy within the umbrella along a neutral level. The evolution of the concentration of tephra particles of a given settling speed v in an axisymmetric intrusion can be modeled using the transport equation [38, 42, 44]

$$\frac{\partial(ch)}{\partial t} + \frac{1}{r}\frac{\partial}{\partial r}(rchu) = -vc, \qquad (1)$$

14

where $c(r,t)$ is the volume concentration of particles, r is the horizontal distance from the plume center, $h(r,t)$ is the thickness of the intrusion, $u(r,t)$ is the thickness-averaged horizontal velocity of the flow, and v is the settling speed of the particle species being considered. The right-hand side represents the rate of particle fallout, which is modeled as proportional to the concentration and the settling speed [38, 44–46]. Time-dependent numerical analysis of the fully time-dependent gravity-current equations [42] shows that the current extends along a near-steady envelope. Consequently, the condition of uniform flux $2\pi rhu \equiv Q$ applies to excellent approximation in Eqn. (1) during the growth of the umbrella. Using this expression to substitute for hu in Eqn. (1) and integrating the resulting equation for c, one obtains the Gaussian prediction for the spatial profile of the mass per unit area of ash deposited per unit time, $m = \rho_b c$ where ρ_b is the density of the basaltic glass, given by

$$m(r) = m_0 e^{-\pi(r/L)^2}, \tag{2}$$

where $L = (Q/v)^{1/2}$ is the umbrella-driven dispersal length scale, and m_0 is the integration constant. The result of (2) applies downstream of the radius of the plume stem, r_0. Assuming that the settling particles are not significantly advected from their fallout position (consistent with the assumption of an approximately quiescent ambient), Eqn. (2) provides the deposition profile of tephra along the seafloor. The constants m_0 and L form the only two parameters defining the dispersal pattern (Eqn. (2)) and describe two independent degrees of freedom associated with purely buoyancy-driven particle dispersal. The constant m_0 represents the accumulation of the dispersal pattern, related to the rate of particle generation and source duration (a larger eruptive duration will accumulate a larger mass per unit area but the dispersal profile will retain the same shape as it accumulates). The parameter L independently represents the radial rate of decay of the deposition pattern, and contains information of the rate of fluid input into the umbrella Q and the settling speed v representing the particle size under consideration. The axisymmetric dispersal pattern described by Eqn. (2) decays monotonically with a smooth tail in all directions from the plume center. With the dispersal length scale L inferred by fitting Eqn. (2) to an observed tephra deposition profile, the volumetric flux feeding the umbrella can then be inferred using the formula

$$Q = vL^2. \tag{3}$$

Since L is independent of both the duration of the eruption and the rate of input of particles (either of which will only accumulate m_0), L independently constrains the information of the volumetric flux sourcing the umbrella via Eqn. (3). Hence, even a small input of particles can, in principle, be sufficient to conduct this inversion. To invert for Q, it remains only estimate the settling speed of the particle under consideration v and the dispersal length L for the observed deposition distribution.

The second step of our inversion predicts the heat energy Φ inputted into the hydrothermal plume at its bed source necessary to produce the volumetric flux Q feeding the umbrella at the top of the stem. The transfer of heat energy, either from inputted hot fluid or heating by lava, produces plume fluid through the process of entrainment of ambient seawater caused by the

15

Symbol	Definition	Value	Source
Q	Volume flux feeding umbrella	2.4 km^3 hour^{-1}	Predicted using Eqn. (3)
L	Buoyancy-driven dispersal length	4.7 km	Fitting Eqn. (2) to data
v	Settling speed for 250-500 µm particles	3 ± 1 cm s^{-1}	Formulae of [33, 34]
Φ	Heat input rate at plume source	3.8×10^{15} J hour^{-1}	Predicted using Eqn. (5)
$\mathcal{F}_0$	Buoyancy flux at plume source	500 m^4 s^{-3}	Predicted above Eqn. (5)
N	Brunt-Väisälä frequency	10^{-3} s^{-1}	WOCE dataset [35]
U	Maximum tidal speed	5 cm s^{-1}	Argo floats [43]
T	Duration of one day	86400 s	
L_{tide}	Tidal dispersal range	700 m	Formula $L_{tide} = UT/2\pi$
τ	Eruption duration	~ 12 hours	Inferred from volume and morphology of lava

Table 1: Parameters with estimated or inferred values.

turbulent upwelling of the plume [3]. To model this, we use the general model for the stem of a convective plume given by [47], as specified by

$$\frac{d\mathcal{Q}}{dz} = a\mathcal{M}^{1/2}, \quad \frac{d\mathcal{M}}{dz} = \frac{\mathcal{F}\mathcal{Q}}{\mathcal{M}}, \quad \frac{d\mathcal{F}}{dz} = -N^2\mathcal{Q}, \tag{4}$$

where z is the vertical coordinate with respect to the seafloor, N is the Brunt-Väisälä frequency, $a = 2\sqrt{\pi}\varepsilon \approx 0.35$ is a dimensionless constant proportional to the entrainment coefficient $\varepsilon \approx 0.1$, and $\mathcal{Q}(z)$, $\mathcal{M}(z)$ and $\mathcal{F}(z)$ are the volume, momentum and buoyancy fluxes, respectively. It should be noted that the model above describes only the predominantly vertically flowing stem of the plume, and does not apply in the neutrally buoyant umbrella for which the earlier model of Eqn. (1) applies. Let $\mathcal{F}_0$ denote the buoyancy flux introduced at the base of the plume. By considering the intrinsic scalings of (4) and $\mathcal{F} \sim \mathcal{F}_0$, we determine the unique intrinsic flux scale in the system as $\mathcal{Q}_* = (a^2\mathcal{F}_0^3/N^5)^{1/4}$. Solving Eqn. (4) numerically using a Runge-Kutta integrator subject to the heat-source condition $\mathcal{F} = \mathcal{F}_0$ and $\mathcal{Q} = \mathcal{M} = 0$ at $z = 0$, we determine further the explicit formula for the flux at the top of the plume $Q = 1.87\mathcal{Q}_* = 1.87\left(a^2\mathcal{F}_0^3/N^5\right)^{1/4}$. This provides the desired relationship between the input of buoyancy at the seafloor $\mathcal{F}_0$ and the flux feeding the umbrella Q. On rearranging this expression for the source buoyancy flux $\mathcal{F}_0$, we obtain $F_0 = 0.87(N^5Q^4)^{1/3}$, which provides the buoyancy flux needed to generate the flux Q at the top of the stem. Applying the physical conversion factor between thermal energy and thermal expansion, we obtain the rate of heat input at the plume stem as

$$\Phi = 0.87\,k\left(Q^4N^5\right)^{1/3}, \tag{5}$$

where $k \equiv \rho c/\alpha g$ is the conversion factor between buoyancy flux and heat flux, ρ is the density of seawater, c is the specific heat capacity, α is the coefficient of thermal expansion, and g is the

acceleration due to gravity. For typical values of $\rho \approx 1027$ kg m^{-3}, $c \approx 4200$ J kg^{-1} K^{-1}, $\alpha \approx 2.1 \times 10^{-4}$ K^{-1} and $g \approx 9.8$ m s^{-2}, the conversion factor takes the value $k \approx 2.1$ GW m^{-4} s^3. Having determined the volumetric flux into the umbrella Q using the first stage of our inversion represented by Eqn. (3), the result of Eqn. (5) provides the flux of heat energy introduced into the plume system at its seafloor origin necessary to produce this flux.

In summary, the general relationships for Q and Φ given by Eqn. (3) and (5) here allow the volumetric flux fed into the umbrella and the rate of heat transfer at the source of the plume to be inferred from observation of the tephra dispersal scale L. Total plume volume V and energy E implied by these relationships are plotted as functions of L in Fig. 4 for an input time scale of $\tau = 12$ hours (estimated for NESCA).

Tidal dispersal

Continuous measurements using flow meters or floats [43], illustrate that tidal currents in the deep oceans form highly regular, symmetrical oscillations superposed with background noise, e.g. from eddies and internal waves. Due to the near-zero time average of tidal velocities over the course of a tidal cycle, both the settling of tephra and advection of the plume system will, under a purely tidal flow field, produce oscillations with a near-zero mean displacement. Hence, the total dispersal by tides is constrained to lie within a certain distance from the source representing the maximum distance a parcel is advected before the tide reverses. Material elements or particles released into a tidal field will undergo periodic, closed orbits in the vicinity of the vent. To illustrate this, we compute the horizontal trajectories of fluid elements or particles, $[x(t), y(t)]$, advected under an illustrative tidal oscillation specified by

$$\dot{x} = U_x \cos(\omega t - \theta_x), \quad \dot{y} = U_y \cos(\omega t - \theta_y), \tag{6}$$

where U_x is the maximum tidal current in the zonal direction, U_y is the maximum tidal current in the meridional direction, ω is the frequency of the tidal oscillation, θ_x and θ_y are phase shifts, and the dot denotes a time derivative. Near the NESCA lava flow, the tidal currents reach magnitudes of approximately 5 cm s^{-1} [43]. To simulate an exemplary tidal pattern, we set $\omega = 4\pi/T$, where T is the duration of one day. Fig. 5a shows the dispersal pattern accumulated following the continuous composition of trajectories of parcels released continuously over the course of one day for an example $U_x = 2\,U_y = 5$ cm s^{-1}, with $\theta_x = t_0\omega$ and $\theta_y = t_0\omega + \pi/2$. The pattern developed by tidal dispersal is confirmed to produce a closed region with an elliptical rim. To determine the rim position for general θ_x, θ_y, U_x and U_y, we integrate (6) subject to the initial release position $(0, 0)$, giving

$$x = \frac{U_x}{\omega} \left[\sin(\omega t - \theta_x) + \sin\theta_x \right], \tag{7}$$

$$y = \frac{U_y}{\omega} \left[\sin(\omega t - \theta_y) + \sin\theta_y \right], \tag{8}$$

describing elliptical trajectories. The rim of the tidal dispersal pattern is the locus of maximum radii arising as t_0 is varied over one tidal cycle. The maximum distance of a particle released at

$t = t_0$ occurs at $t = t_0 + \pi/\omega$. Substituting this value into (7) and (8), we determine the rim position parametrised as a function of t_0, given by

$$R(t_0) = \frac{2}{\omega} \left[U_x^2 \cos^2(\omega t_0) + U_y^2 \cos^2(\omega t_0 - \Delta\theta) \right]^{1/2},$$ (9)

where $\theta_x = \omega t_0$ and $\Delta\theta = \theta_y - \omega t_0$. The maximum dispersal distance is thus bounded by $L_{tide} = 2U/\omega = UT/2\pi$, where U is the larger of U_x and U_y. Mixed diurnal and semi-diurnal patterns can be modeled by superposition of two patterns of the form (6) with one frequency twice the other. This results in more complex patterns than purely elliptical, but are likewise constrained by the maximum tidal distance of L_{tide}, with U the maximum tidal speed in any given direction. For typical tidal currents in the NESCA region estimated from Argo floats [43], $U \lesssim 5$ cm s^{-1}, and hence $L_{tide} \lesssim 0.7$ km. In the absence of buoyancy-driven expansion of the umbrella, the independent effect of tides is thus to advect the plume-particle system back and forth within a radius of oscillation L_{tide}.

In addition to the closure of the orbit, a notable characteristic of purely tidal dispersal is the development of a sharp local maximum at the 'rim' of the tephra deposition pattern, evident in Fig. 5a (at least for a pure diurnal or semi-diurnal pat ern; mixed tides, as apply in the NE Pacific, will produce a more complex pattern, though a similar constraint on the orbit will apply). This phenomenon is a consequence of the lingering of the trajectories near the rim as they switch direction during tidal reversal. Another characteristic is the non-axisymmetric eccentricity of the tidal dispersal pattern, which will generally arise for $U_x \neq U_y$ and $\theta_x \neq \theta_y$.

The deposition of tephra around the NESCA lava of more than 5 km in all directions is considerably larger than the maximum tidal dispersal scale $L_{tide} \sim 0.7$ km. In view of this, tidal advection cannot account for the observed deposition pattern at NESCA. Thus, we propose that the dispersal was instead driven predominantly by buoyancy-driven radial flow of the intrusion along the neutral level.

Polydisperse deposition

Eqn. (3) provides the volumetric flux feeding the megaplume as a function of the dispersal scale L for a monodisperse distribution with settling speed $\sim v$. For a polydisperse distribution of particles, the total deposited mass per unit area $M(r)$ at a radius r can be represented by the weighted superposition

$$M(r) = \int_0^\infty R_0(\tilde{v}) c_0(\tilde{v}) \mathrm{e}^{-\pi[r/L(\tilde{v})]^2} \, \mathrm{d}\tilde{v},$$ (10)

where $R(\tilde{v})$ is the mass per particle with settling speed $\tilde{v}$, and $c_0(\tilde{v})$ and $L(\tilde{v})$ are distributions representing the number density of particles with settling speed $\tilde{v}$ and the dispersal range of the particles with settling speed $\tilde{v}$, respectively. To conduct the inversion for Q using (3), we begin by choosing a particle range $[d - \delta d/2, d + \delta d/2]$, where d is the center value of the group and δd
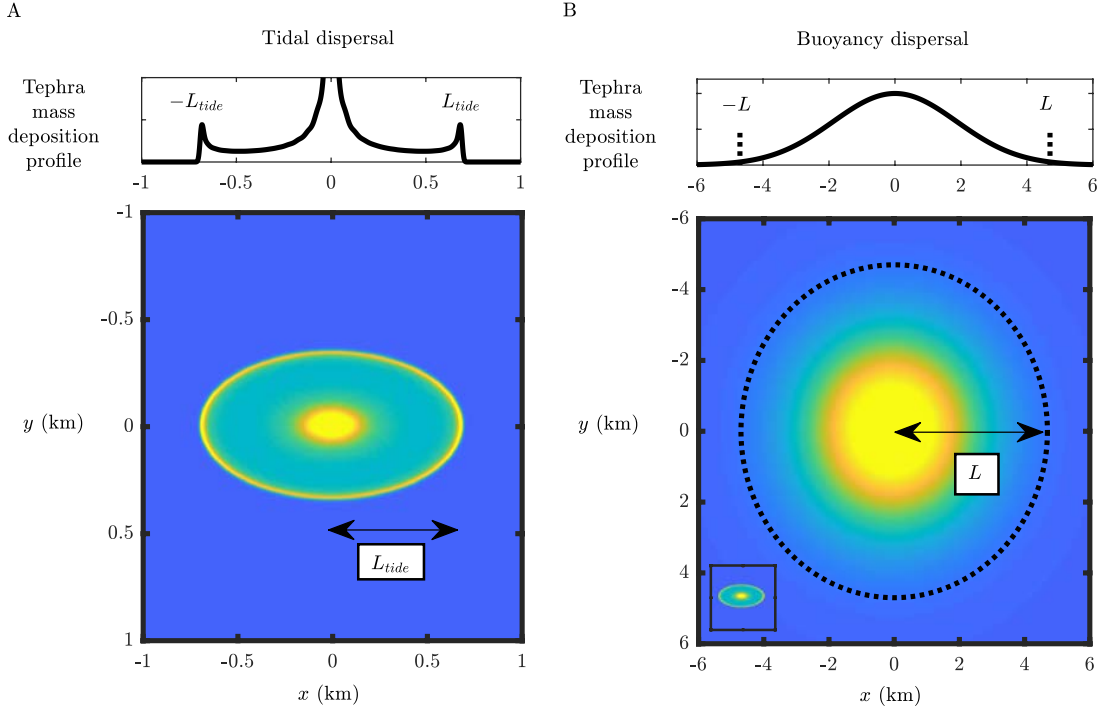
Figure 5: **Plan-views of the typical tephra deposition fields produced by tides or by buoyancy-driven lateral transport in the umbrella of the hydrothermal plume.** A characteristic dispersal field from (A) tidal advection and (B) advection within a buoyancy-driven umbrella, representing two end members for submarine tephra dispersal. Blue represents no particles, while yellow represents maximal deposited concentration. The tidal pattern (a) is given by superposing trajectories of particles released continuously over the course of one day predicted by the kinematic model of Eqn. (6), showing the maximum dispersal distance of L_{tide} by tidal oscillation. The buoyancy-driven pattern (b) is given by the prediction of Eqn. (2). The case $L = 4.7$ km is illustrated for (b), corresponding to the dispersal distance inferred by fitting the deposition profiles for NESCA (Fig. 2). Upper panels show cross-sections of the dispersal patterns, illustrating the fundamentally different decay characteristics and dispersal distances operating under the two mechanisms. Panel (b) shows the tidal dispersal on the same scale as an inset, illustrating its considerably smaller scale.

is the size range within the group, and associated range of settling speeds $[v - \delta v/2, v + \delta v/2]$.
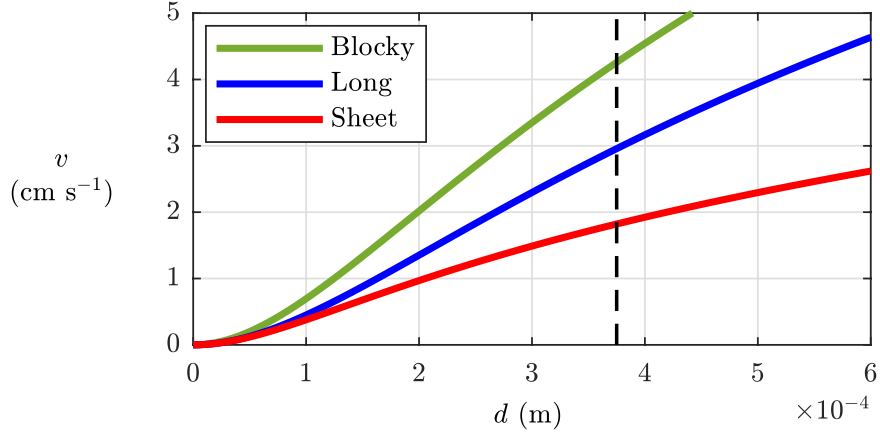
Figure 6: **Settling speed as a function of pyroclastic particle size.** The settling speed v of three different types of clast are plotted against the particle size d, as predicted by the formula of [33] with the coefficients for basaltic tephra determined from tank experiments by [34]. The relationships are used to determine the characteristic settling speeds of the particles in the 250-500 µm range used to conduct our inversion for the volumetric flux of fluid fed into the umbrella through Eqn. (3).

The mass per unit area of particles in this group is given by

$$m(r) = \int_{v-\delta v/2}^{v+\delta v/2} R(\tilde{v})c_0(\tilde{v})e^{-\pi[r/L(\tilde{v})]^2}\,\mathrm{d}\tilde{v} \tag{11}$$

$$= m_0 e^{-\pi(r/L)^2} \tag{12}$$

where $m_0 \approx \delta v R(v)c_0(v)$. The dispersal scale L can then be determined by applying a least-squares fit between Eqn. (12) and dispersal data for particles in the size range $[d - \delta d/2, d + \delta d/2]$, with m_0 and L treated as fitting parameters. Doing this for each of the three profiles of particles in the range $d = 250$–500 µm from the data of [10], we inferred the value $L \approx 4.7$ km for a consistent radial origin proximal to the center of the lava flow (shown as a yellow star in the map of Fig. 2).

Particle settling speeds

In order to determine a representative settling speed for this category, we utilized the relationship of [33] incorporating the coefficients for pyroclastic shapes determined using tank experiments by [34] (see Fig. 6). For the size range 250-500 µm used in our inversion (corresponding to the deposition shown in Fig. 2), the range $v = 3 \pm 1$ cm s^{-1} is representative.
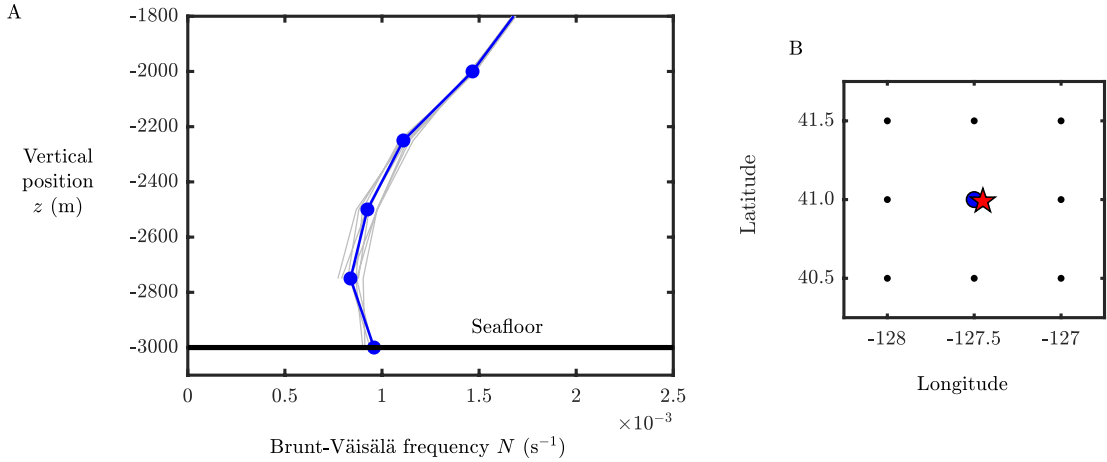
Figure 7: **Profile of the Brunt-Väisälä frequency** N **as a function of height from the seafloor.** The profiles are provided by the dataset of [35]. Panel (A) shows the profile of $N = [-(g/\rho_0)\partial\rho/\partial z]^{1/2}$ as a function of vertical position, where $g \approx 9.8$ m s^{-2} and $\rho_0 \approx 1027$ kg m^{-3}. The profile for the horizontal coordinate closest to the NESCA lava flow is shown as a blue curve. Profiles for the 8 surrounding profiles a distance of 0.5 degrees away are shown as gray curves. Panel (B) shows a plan-view of the sampled coordinates, with the position of the NESCA lava flow indicated by the red star. The data point position closest to the lava flow is shown as a blue circle and corresponds with the blue curve in panel A. The eight surrounding Argo positions are shown as black dots. The plot is used to infer a characteristic value of $N \approx 10^{-3}$ s^{-1} for the abyssal ocean in this region, used for the inversion for the rate of heat transfer Φ in Eqn. (5).

Ocean density stratification

The vertical profile of the Brunt-Väisälä frequency N from the seafloor near the NESCA site is shown in Fig. 7A, derived using the dataset derived from ARGO floats [35]. The profile corresponds to the data gathered at the data point, shown as a blue circle in panel B, which lies closest to the lava flow. This and the 8 surrounding profiles (shown as black dots in panel B), produce a similar value $N \approx 10^{-3}$ s^{-1} for the abyssal region.

Reaching the umbrella

The considerable dispersal of tephra that occurs during a submarine eruption relies on an appreciable proportion of the ash particles being transported to the umbrella. This appendix derives a theoretical condition dependent on an associated dimensionless number for the ash to undergo transportation into, and dispersal by, the umbrella. This is done first by considering a neces-

sary condition for significant umbrella dispersal, namely, that the dispersal distance predicted by the intrusion dynamics is considerable larger than the radius of the plume stem. Second, we determine the characteristic 'rise height' of particles in the plume and, by comparing this to the neutral level of the plume, determine a condition for a significant proportion of particles to reach the umbrella. The two conditions derived are found to involve the same key dimensionless parameter grouping $v^4/(NF_0)$, showing that this number independently indexes the relative significance of stem fallout to umbrella fallout.

In accordance with the top-hat form of the model of [47], the radius of the plume stem satisfies $r = Q^2/M$. The characteristic maximum radius can then be evaluated as

$$r_0 \sim 0.7\, a\mathcal{H} = 0.1H, \tag{13}$$

where $\mathcal{H} = (F_0/N^3)^{1/4}$ is the intrinsic height scale (obtained from scaling analysis of Eqn.s (4) with $F \sim F_0$) and $H \approx 4.3\,\mathcal{H}$ is the rise height. The rise height of a plume in a uniform stratification is therefore ten times the radius of the stem at the neutral level. The radius r_0 represents the characteristic maximum possible distance that can be dispersed by the stem. Thus, if tephra is observed to have spread radially from a source at a distance appreciably greater than r_0, then the particle must have entered the umbrella (under our assumption of a quiescent ambient). By considering the ratio of r_0 to the length scale associated with umbrella-driven dispersal L in Eqn. (2), we derive the dimensionless number

$$\Lambda \equiv L/r_0, \tag{14}$$

which characterizes the ratio of umbrella dispersal to maximum stem dispersal. A condition for significant umbrella dispersal of a particle species with settling speed v is that $\Lambda \gg 1$. On the other hand, stem fallout will be dominant for this species if $\Lambda \ll 1$. Thus, Λ can be used as a metric for characterizing the source strength necessary for umbrella dispersal. Substituting for the rise height using the result $H = 4.3\mathcal{H}$ and for the flux reaching the umbrella using our prediction $Q = 1.1\mathcal{Q}_c$, where $\mathcal{Q}_c \equiv (F_0^3/N^5)^{1/4}$ noted after Eqn. (4), we obtain

$$\Lambda = \frac{10\sqrt{Q/v}}{H} = 2.4 \left(\frac{F_0 N}{v^4}\right)^{\frac{1}{8}}, \tag{15}$$

where we have used the expressions for the flux at the top of the plume stem and the rise height to substitute for Q and H in the second equality. For values of $F_0 \approx 500$ m^4 s^{-3}, $N \approx 10^{-3}$ s^{-1} and $v \approx 3$ cm s^{-1} arising in our analysis of the NESCA eruption, $\Lambda \approx 13 \gg 1$. This prediction reinforces our hypothesis that the umbrella of the plume was responsible for driving the dispersal to the observed distances.

From the perspective of the plume stem, a necessary condition for significant umbrella dispersal to occur is that a significant number of particles introduced into the stem of the plume reach the height of the umbrella. The dispersal produced by the stem of a plume was considered by [51] for the case of a uniform-density ambient fluid. Here, we consider the different case of

an ambient stratification with constant Brunt-Väisälä frequency N. Following [51], we describe the volume concentration distribution of particles in the stem of the plume using the equation

$$\frac{\partial}{\partial t}(Ac) + \frac{\partial}{\partial x}(\mathcal{Q}c) = -v(2\pi r)c, \tag{16}$$

where A is the horizontal cross-sectional area of the plume (defined as $A = \mathcal{Q}^2/\mathcal{M}$ in the top-hat version of the model of [47]), $r = \sqrt{A/\pi}$ is the plume radius, $c(z,t)$ is the cross-sectionally averaged particle concentration and $\mathcal{Q}$ is the volume flux of the plume, as governed by Eqn. (4). For the established steady flow, the integration of Eqn. (16) yields

$$c(z) = \frac{K}{\mathcal{Q}(z)} \exp\left[-2\sqrt{\pi}v \int_0^z \mathcal{M}(\tilde{z})^{-1/2}\, \mathrm{d}\tilde{z}\right], \tag{17}$$

where K is the constant of integration representing the particle-concentration flux inputted at the source. The result above provides the vertical distribution of particles in a steady plume for any given plume solution. The intrinsic vertical scale of this concentration distribution is determined by the decay scale of the exponential. We can determine the characteristic rise height of particles as the height z for which

$$2\sqrt{\pi}v \int_0^z \mathcal{M}(\tilde{z})^{-1/2}\, \mathrm{d}\tilde{z} \approx 10. \tag{18}$$

A good approximation for the momentum-flux profile given by Eqn. (4) between the source and the neutral level is $\mathcal{M} \approx 0.3(F_0/N)z/\mathcal{H}$. Substituting this approximation into Eqn. (18), we obtain the expression for the characteristic particle rise height z_* as

$$z_* \sim 0.6 \left(\frac{F_0^3}{Nv^8}\right)^{1/4}. \tag{19}$$

The ratio of this particle rise height to the neutral level of the plume is

$$\frac{z_*}{3.3\,\mathcal{H}} = 1.8 \left(\frac{F_0 N}{v^4}\right)^{1/4}. \tag{20}$$

The dimensionless number v^4/NF_0 has, as in Eqn. (15), again appeared as the key dimensionless number that controls the propensity for a given particle species with settling speed v to undergo primarily stem versus umbrella dispersal. If $v^4/NF_0 \ll 1$, the particles will reach the umbrella and be dispersed primarily by the intrusion to form the guassian deposition profile given by Eqn. (2) with a horizontal dispersal length scale of $O(L)$. If $v^4/NF_0 \gg 1$, particles will fail to reach the umbrella, and will instead settle from the stem within a distance of $O(r_0)$ or less from the stem source.

References

[1] White, J. D., Smellie, J. L. & Clague, D. A. Introduction: A deductive outline and topical overview of subaqueous explosive volcanism. *Explosive subaqueous volcanism* **140**, 1–23 (2003).

[2] Baker, E. T., Massoth, G. J. & Feely, R. A. Cataclysmic hydrothermal venting on the Juan de Fuca Ridge. *Nature* **329**, 149 (1987).

[3] Baker, E. *et al.* Episodic venting of hydrothermal fluids from the Juan de Fuca Ridge. *Journal of Geophysical Research: Solid Earth* **94**, 9237–9250 (1989).

[4] Embley, R., Chadwick, W., Perfit, M. & Baker, E. Geology of the northern Cleft segment, Juan de Fuca Ridge: Recent lava flows, sea-floor spreading, and the formation of megaplumes. *Geology* **19**, 771–775 (1991).

[5] Baker, E. T. *et al.* Hydrothermal discharge during submarine eruptions: The importance of detection, response, and new technology. *Oceanography* **25**, 128–141 (2012).

[6] Baker, E. T. *et al.* Unique event plumes from a 2008 eruption on the Northeast Lau Spreading Center. *Geochemistry, Geophysics, Geosystems* **12** (2011).

[7] Lupton, J. E., Baker, E. T. & Massoth, G. J. Helium, heat, and the generation of hydrothermal event plumes at mid-ocean ridges. *Earth and Planetary Science Letters* **171**, 343–350 (1999).

[8] Palmer, M. R. & Ernst, G. G. J. Generation of hydrothermal megaplumes by cooling of pillow basalts at mid-ocean ridges. *Nature* **393**, 643 (1998).

[9] Lowell, R. P. & Germanovich, L. N. Dike injection and the formation of megaplumes at ocean ridges. *Science* **267**, 1804–1807 (1995).

[10] Clague, D. A., Paduan, J. B. & Davis, A. S. Widespread strombolian eruptions of mid-ocean ridge basalt. *Journal of Volcanology and Geothermal Research* **180**, 171–188 (2009).

[11] Lavelle, J. The initial rise of a hydrothermal plume from a line segment source: Results from a three-dimensional numerical model. *Geophysical research letters* **22**, 159–162 (1995).

[12] Summit, M. & Baross, J. A. Thermophilic subseafloor microorganisms from the 1996 North Gorda Ridge eruption. *Deep Sea Research Part II: Topical Studies in Oceanography* **45**, 2751–2766 (1998).

[13] Embley, R. W. & Lupton, J. E. Diking, event plumes, and the subsurface biosphere at mid-ocean ridges. *Washington DC American Geophysical Union Geophysical Monograph Series* **144**, 75–97 (2004).

[14] Clague, D. A., Davis, A. S. & Dixon, J. E. Submarine strombolian eruptions on the gorda mid-ocean ridge. *Explosive subaqueous volcanism* **140**, 111–128 (2003).

[15] Sohn, R. A. *et al.* Explosive volcanism on the ultraslow-spreading Gakkel Ridge, Arctic Ocean. *Nature* **453**, 1236 (2008).

[16] Clague, D. A., Davis, A. S., Bischoff, J. L., Dixon, J. E. & Geyer, R. Lava bubble-wall fragments formed by submarine hydrovolcanic explosions on Lō'ihi Seamount and Kīlauea Volcano. *Bulletin of Volcanology* **61**, 437–449 (2000).

[17] Batiza, R., Fornari, D. J., Vanko, D. A. & Lonsdale, P. Craters, calderas, and hyaloclastites on young pacific seamounts. *Journal of Geophysical Research: Solid Earth* **89**, 8371–8390 (1984).

[18] Portner, R. A., Clague, D. A., Helo, C., Dreyer, B. M. & Paduan, J. B. Contrasting styles of deep-marine pyroclastic eruptions revealed from Axial Seamount push core records. *Earth and Planetary Science Letters* **423**, 219–231 (2015).

[19] Ferguson, D. J. *et al.* A 65 k.y. time series from sediment-hosted glasses reveals rapid transitions in ocean ridge magmas. *Geology* **45**, 491–494 (2017).

[20] Lund, D. C. *et al.* Anomalous Pacific-Antarctic Ridge volcanism precedes glacial termination 2. *Geochemistry, Geophysics, Geosystems* **19**, 2478–2491 (2018).

[21] Eissen, J.-P., Fouquet, Y., Hardy, D. & Ondréas, H. Recent morb volcaniclastic explosive deposits formed between 500 and 1750 mbsl on the axis of the mid-atlantic ridge, south of the azores. *Washington DC American Geophysical Union Geophysical Monograph Series* **140**, 143–166 (2003).

[22] Maicher, D. & White, J. D. The formation of deep-sea Limu o Pele. *Bulletin of Volcanology* **63**, 482–496 (2001).

[23] Ross, S. L. & Zierenberg, R. A. Volcanic geomorphology of the SESCA and NESCA sites, Escanaba Trough. *Geologic, hydrothermal, and biologic studies at Escanaba Trough, Gorda Ridge, offshore northern California. US Geol. Surv. Bull* **2022**, 143–151 (1994).

[24] Murch, A. P., White, J. D. & Carey, R. J. Characteristics and deposit stratigraphy of submarine-erupted silicic ash, Havre volcano, Kermadec Arc, New Zealand. *Frontiers in Earth Science* **7**, 1 (2019).

[25] Walker, S. L. *et al.* Eruption-fed particle plumes and volcaniclastic deposits at a submarine volcano: NW Rota-1, Mariana Arc. *Journal of Geophysical Research: Solid Earth* **113** (2008).

[26] Carey, R. *et al.* The largest deep-ocean silicic volcanic eruption of the past century. *Science advances* **4**, e1701121 (2018).

[27] Chadwick Jr, W. *et al.* Direct video and hydrophone observations of submarine explosive eruptions at NW Rota-1 Volcano, Mariana Arc. *Journal of Geophysical Research: Solid Earth* **113** (2008).

[28] Deardorff, N. D., Cashman, K. V. & Chadwick Jr, W. W. Observations of eruptive plume dynamics and pyroclastic deposits from submarine explosive eruptions at NW Rota-1, Mariana Arc. *Journal of Volcanology and Geothermal Research* **202**, 47–59 (2011).

[29] Resing, J. A. *et al.* Active submarine eruption of boninite in the northeastern lau basin. *Nature Geoscience* **4**, 799–806 (2011).

[30] Head III, J. W. & Wilson, L. Deep submarine pyroclastic eruptions: theory and predicted landforms and deposits. *Journal of Volcanology and Geothermal Research* **121**, 155–193 (2003).

[31] Baker, E. T. *et al.* Hydrothermal event plumes from the CoAxial seafloor eruption site, Juan de Fuca Ridge. *Geophysical Research Letters* **22**, 147–150 (1995).

[32] Bonadonna, C. & Phillips, J. C. Sedimentation from strong volcanic plumes. *Journal of Geophysical Research: Solid Earth* **108** (2003).

[33] Ferguson, R. & Church, M. A simple universal equation for grain settling velocity. *Journal of Sedimentary Research* **74**, 933–937 (2004).

[34] Barreyre, T., Soule, S. A. & Sohn, R. A. Dispersal of volcaniclasts during deep-sea eruptions: Settling velocities and entrainment in buoyant seawater plumes. *J. Vol. and Geo. Res.* **205**, 84–93 (2011).

[35] Gouretski, V. & Koltermann, K. P. WOCE Global Hydrographic Climatology. *Berichte des BSH* **35**, 1–52 (2004).

[36] Colombier, M. *et al.* In situ granulation by thermal stress during subaqueous volcanic eruptions. *Geology* **47**, 179–182 (2019).

[37] D'Asaro, E., Walker, S. & Baker, E. Structure of two hydrothermal megaplumes. *Journal of Geophysical Research: Oceans* **99**, 20361–20373 (1994).

[38] Sparks, R. S. J., Carey, S. N. & Sigurdsson, H. Sedimentation from gravity currents generated by turbulent plumes. *Sedimentology* **38**, 839–856 (1991).

[39] Carey, S. & Sparks, R. S. J. Quantitative models of the fallout and dispersal of tephra from volcanic eruption columns. *Bulletin of Volcanology* **48**, 109–125 (1986).

[40] Bonadonna, C. *et al.* Probabilistic modeling of tephra dispersal: Hazard assessment of a multiphase rhyolitic eruption at Tarawera, New Zealand. *Journal of Geophysical Research: Solid Earth* **110** (2005).

[41] Barsotti, S., Neri, A. & Scire, J. S. The VOL-CALPUFF model for atmospheric ash dispersal: 1. Approach and physical formulation. *Journal of Geophysical Research: Solid Earth* **113** (2008).

[42] Johnson, C. G. *et al.* Modelling intrusions through quiescent and moving ambients. *Journal of Fluid Mechanics* **771**, 370406 (2015).

[43] Ollitrault, M. & Rannou, J.-P. Andro: An Argo-based deep displacement dataset. *Journal of Atmospheric and Oceanic Technology* **30**, 759–788 (2013).

[44] Sutherland, B. R. & Hong, Y. S. D. Sedimentation from particle-bearing plumes in a stratified ambient. *Phys. Rev. Fluids* **1**, 074302 (2016).

[45] Hazen, A. On sedimentation. *Transactions of the American Society of Civil Engineers* **54**, 45–88 (1904).

[46] Martin, D. & Nokes, R. Crystal settling in a vigorously convecting magma chamber. *Nature* **332**, 534–536 (1988).

[47] Morton, B. R., Taylor, G. I. & Turner, J. S. Turbulent gravitational convection from maintained and instantaneous sources. *Proc. R. Soc. Lond. A* **234**, 1–23 (1956).

[48] Griffiths, R. W. & Fink, J. H. Solidification and morphology of submarine lavas: A dependence on extrusion rate. *Journal of Geophysical Research: Solid Earth* **97**, 19729–19737 (1992).

[49] Gregg, T. K. & Fornari, D. J. Long submarine lava flows: Observations and results from numerical modeling. *Journal of Geophysical Research: Solid Earth* **103**, 27517–27531 (1998).

[50] Xu, G., Chadwick Jr, W. W., Wilcock, W. S., Bemis, K. G. & Delaney, J. Observation and modeling of hydrothermal response to the 2015 eruption at Axial Seamount, Northeast Pacific. *Geochemistry, Geophysics, Geosystems* **19**, 2780–2797 (2018).

[51] Ernst, G. G. J., Sparks, R. S. J., Carey, S. N. & Bursik, M. I. Sedimentation from turbulent jets and plumes. *Journal of Geophysical Research: Solid Earth* **101**, 5575–5589 (1996).